

New method of precise measurement of positronium hyperfine splitting

A. Ishida^{a,*}, G. Akimoto^a, Y. Sasaki^a, T. Suehara^b, T. Namba^b, S. Asai^a, T. Kobayashi^b, H. Saito^c, M. Yoshida^d, K. Tanaka^d, and A. Yamamoto^d

^a*Department of Physics, Graduate School of Science, The University of Tokyo, 7-3-1 Hongo, Bunkyo-ku, Tokyo 113-0033, Japan*

^b*International Center for Elementary Particle Physics (ICEPP), The University of Tokyo, 7-3-1 Hongo, Bunkyo-ku, Tokyo 113-0033, Japan*

^c*Department of General Systems Studies, Graduate School of Arts and Sciences, The University of Tokyo, 3-8-1 Komaba, Meguro-ku, Tokyo 153-8902, Japan*

^d*High Energy Accelerator Research Organization (KEK), 1-1 Oho, Tsukuba, Ibaraki 305-0801, Japan*

Abstract

The ground state hyperfine splitting of positronium, Δ_{HFS} , is sensitive to high order corrections of QED. A new calculation up to $O(\alpha^3 \ln \alpha)$ has revealed a 3.9σ discrepancy between the QED prediction and the experimental results. This discrepancy might either be due to systematic problems in the previous experiments or to contributions beyond the Standard Model. We propose an experiment to measure Δ_{HFS} employing new methods designed to remedy the systematic errors which may have affected the previous experiments. Our experiment will provide an independent check of the discrepancy. The prototype run has been finished and a result of $\Delta_{\text{HFS}} = 203.380\,4 \pm 0.008\,4$ GHz (41 ppm) has been obtained. A measurement with a precision of $O(\text{ppm})$ is expected within a few years.

Keywords: quantum electrodynamics (QED), positronium, hyperfine splitting (HFS)

1. Introduction

Positronium (Ps), a bound state of an electron and a positron, is a purely leptonic system which allows for very sensitive tests of Quantum ElectroDynamics (QED). The precise measurement of the hyperfine splitting between orthopositronium (o-Ps, 1^3S_1) and parapositronium (p-Ps, 1^1S_0) (Ps-HFS) provides a good test of bound state QED. Ps-HFS is expected to be relatively large (for example compared to hydrogen HFS) due to a relatively large spin-spin interaction, and also due to the contribution from vacuum oscillation (o-Ps $\rightarrow \gamma^* \rightarrow$ o-Ps). The contribution from vacuum oscillation is sensitive to new physics beyond the Standard Model.

Figure 1 shows the measured and theoretical values of Ps-HFS. The combined value from the results of the previous 2 experiments is $\Delta_{\text{HFS}}^{\text{exp}} = 203.388\,65(67)$ GHz (3.3 ppm) [1, 2]. Recent developments in NonRelativistic QED (NRQED) have added $O(\alpha^3 \ln \alpha)$ corrections to the theoretical prediction which now stands at $\Delta_{\text{HFS}}^{\text{th}} = 203.391\,69(41)$ GHz (2.0 ppm) [3]. The discrepancy of $3.04(79)$ MHz (15 ppm, 3.9σ) between $\Delta_{\text{HFS}}^{\text{exp}}$ and $\Delta_{\text{HFS}}^{\text{th}}$ might either be due to the common systematic uncertainties in the previous experiments or to new physics beyond the Standard Model.

There are two possible common systematic uncertainties in the previous experiments. One is the unthermalized o-Ps contribution which results in an underestimation of the material effect. This effect has already been shown to be significant [4, 5, 6] in the o-Ps lifetime puzzle. The other is the uncer-

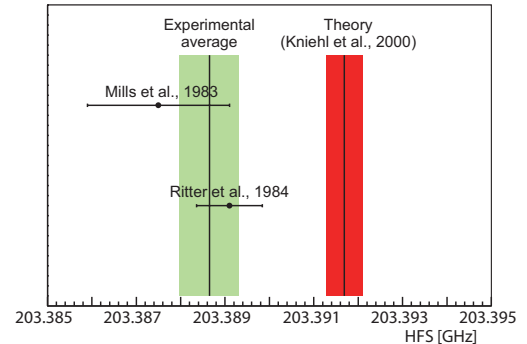


Figure 1: Measured and theoretical values of Ps-HFS.

tainty in the magnetic field uniformity which was cited as the most significant systematic error by previous experimenters.

2. Theory of Experiment

2.1. Measurement using Zeeman effect

The energy levels of the ground state of Ps are shown as a function of static magnetic field in Figure 2. Due to technical difficulties in directly stimulating Δ_{HFS} , we make an indirect measurement by stimulating the transition Δ_{mix} . This is the same approach as previous experiments. The relationship between Δ_{HFS} and Δ_{mix} is approximately given by the Breit-Rabi equation

$$\Delta_{\text{mix}} \simeq \frac{1}{2} \Delta_{\text{HFS}} \left(\sqrt{1 + 4x^2} - 1 \right), \quad (1)$$

*Corresponding author (TEL:+81-3-3815-8384 / FAX:+81-3-3814-8806)
Email address: ishida@icepp.s.u-tokyo.ac.jp (A. Ishida)

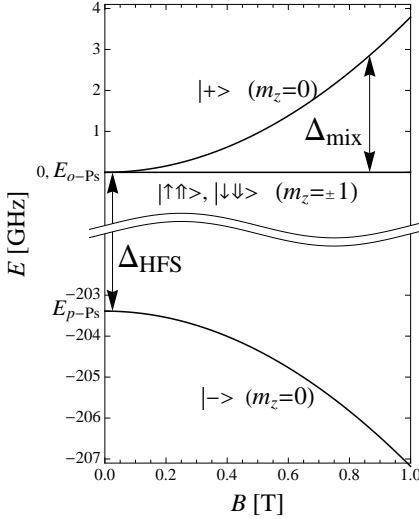


Figure 2: Zeeman energy levels of Ps in its ground state. The arrows \uparrow, \downarrow means the spin up and down of electron, and the arrows $\uparrow\uparrow, \downarrow\downarrow$ means the spin up and down of positron.

in which $x = g'\mu_B B / h\Delta_{\text{HFS}}$, $g' = g \left(1 - \frac{5}{24}a^2\right)$ is the g factor for a positron (electron) in Ps [7], μ_B is the Bohr magneton, B is the static magnetic field, and h is the Plank constant.

In a static magnetic field, the $|S, m_z\rangle = |0, 0\rangle$, where S is the total spin of Ps and m_z is the magnetic quantum number of Ps along with z-axis (direction of static magnetic field), state mixes with the $|1, 0\rangle$ state hence the $|+\rangle$ state annihilates into 2 γ -rays with a lifetime of about 8 ns (with our experimental conditions). The $|1, \pm 1\rangle$ states annihilate into 3 γ -rays with a lifetime of about 140 ns. When a microwave field with a frequency of Δ_{mix} is applied, transitions between the $|+\rangle$ state and the $|1, \pm 1\rangle$ states are induced so that the 2 γ -ray annihilation rate increases and the 3 γ -ray annihilation rate decreases. This change of annihilation rates is our experimental signal.

Our experimental resonance line shape is obtained using density matrix. We use the basis for four spin eigenstates of Ps as $(\psi_0, \psi_1, \psi_2, \psi_3) \equiv (|0, 0\rangle, |1, 0\rangle, |1, 1\rangle, |1, -1\rangle)$. We apply a magnetic field

$$\mathbf{B}(t) = B\mathbf{e}_z + B_0\mathbf{e}_x \cos(\omega t), \quad (2)$$

where $\mathbf{e}_z, \mathbf{e}_x$ are the unit vectors for z, x direction respectively, B_0 is magnetic field strength of microwaves, and ω is the frequency of microwaves. Then the Hamiltonian \mathbf{H} becomes

$$\mathbf{H} = \begin{pmatrix} -\frac{1}{2} - \frac{1}{2}\gamma_s & x & -y & y \\ x & \frac{1}{2} - \frac{1}{2}\gamma_t & 0 & 0 \\ -y & 0 & \frac{1}{2} - \frac{1}{2}\gamma_t & 0 \\ y & 0 & 0 & \frac{1}{2} - \frac{1}{2}\gamma_t \end{pmatrix} h\Delta_{\text{HFS}}, \quad (3)$$

where $y = C_y \frac{g'\mu_B B_0}{h\Delta_{\text{HFS}}} \cos(\omega t)$, C_y is a constant, $\gamma_s = \frac{\Gamma_{\text{p-Ps}}}{2\pi\Delta_{\text{HFS}}}$, $\gamma_t = \frac{\Gamma_{\text{o-Ps}}}{2\pi\Delta_{\text{HFS}}}$, $\Gamma_{\text{p-Ps}}$ is the decay rate of p-Ps, and $\Gamma_{\text{o-Ps}}$ is that of o-Ps. The most recent and precise experimental values are $\Gamma_{\text{o-Ps}} = 7.0401(7)\mu\text{s}^{-1}$ [4] and $\Gamma_{\text{p-Ps}} = 7.9909(17)\text{ns}^{-1}$ [8].

From the time-dependent Schrödinger equation, the 4×4 density matrix $\rho(t)$ is given by

$$i\hbar\dot{\rho} = \mathbf{H}\rho - \rho\mathbf{H}^\dagger, \quad (4)$$

where the i, j -element of $\rho(t)$ is defined as $\rho_{ij}(t) \equiv \langle \psi_i | \psi(t) \rangle \langle \psi(t) | \psi_j \rangle$. If we take the initial state to be unpolarized, $\rho(0) = \text{diag}\left(\frac{1}{4}, \frac{1}{4}, \frac{1}{4}, \frac{1}{4}\right)$.

The 2γ -ray annihilation probability $S_{2\gamma}$ and 3γ -ray annihilation probability $S_{3\gamma}$, between $t = t_0$ and $t = t_1$, are obtained by

$$S_{2\gamma} = \Gamma_{\text{p-Ps}} \int_{t_0}^{t_1} \rho_{00}(t) dt, \quad (5)$$

$$S_{3\gamma} = \Gamma_{\text{o-Ps}} \int_{t_0}^{t_1} (\rho_{11}(t) + \rho_{22}(t) + \rho_{33}(t)) dt. \quad (6)$$

2.2. Ps Thermalization Effect

Forming Ps needs material to provide electrons, but material around Ps makes electric field and changes Δ_{HFS} . This effect is called the Stark effect. The material effect must be properly considered to evaluate Δ_{HFS} in vacuum. In the previous experiments, the material effect on Δ_{HFS} was considered to be proportional to the material (gas) density. Δ_{HFS} was measured at various gas density, and they were extrapolated linearly to zero density [1, 2]. But this extrapolation method can make large systematic error enough to account for the discrepancy between $\Delta_{\text{HFS}}^{\text{exp}}$ and $\Delta_{\text{HFS}}^{\text{th}}$.

Formed Ps has the initial energy of O(eV). Positronium loses its energy when it collides with material, and finally its energy becomes to room temperature ($\sim 1/30$ eV). This process is called thermalization. The material effect between $t = t_0$ and $t = t_1$ is proportional to

$$\int_{t_0}^{t_1} f(t) (\rho_{00}(t)(B_0 \neq 0) - \rho_{00}(t)(B_0 = 0)) dt, \quad (7)$$

where $f(t) \sim n\sigma v(t)$ is the collision rate of Ps with material, n is the number density of material, σ is the typical cross section of collision, and $v(t)$ is the mean velocity of Ps. In the previous experiments, timing information was not measured so that $t_0 = 0$ and $t_1 = \infty$. The effect is proportional to the material density if the thermalization occurs much faster than the o-Ps lifetime, but the thermalization time scale becomes large especially at low material density, which makes nonlinear effect on Δ_{HFS} .

The nonlinear effect can be estimated using the thermalization model [9],

$$\frac{dE_{\text{av}}(t)}{dt} = -\sqrt{2m_{\text{Ps}}E_{\text{av}}(t)} \left(E_{\text{av}}(t) - \frac{3}{2}kT \right) \frac{8}{3} \sqrt{\frac{2}{3\pi}} \frac{2\sigma_m n}{M}, \quad (8)$$

where $E_{\text{av}}(t)$ is the average Ps energy, m_{Ps} is the Ps mass, M is the mass of the gas molecule, T is the temperature of the gas, k is the Boltzmann constant, and $\frac{8}{3} \sqrt{\frac{2}{3\pi}} \frac{2\sigma_m n}{M}$ means the collision effect. The solution of this equation is [10]

$$E_{\text{av}}(t) = \left(\frac{1 + Ae^{-bt}}{1 - Ae^{-bt}} \right)^2 \frac{3}{2}kT, \quad (9)$$

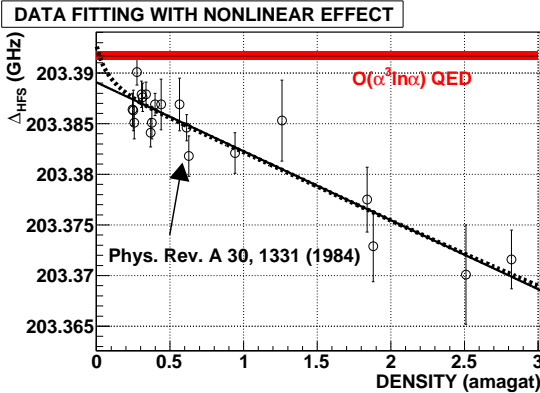


Figure 3: (Color online) Thermalization effect on Δ_{HFS} . The circles and error bars are the data of Ref. [1], the solid line is the linear fit, the dashed line is the best fit including Ps thermalization effect, and the red band is the $O(\alpha^3 \ln \alpha)$ QED prediction in vacuum.

where $b = \frac{8}{3} \sqrt{\frac{2}{3\pi}} \frac{2\sigma_m n}{M} \sqrt{3m_{\text{Ps}} kT}$, $A = \frac{\sqrt{E_0} - \sqrt{\frac{3}{2} kT}}{\sqrt{E_0} + \sqrt{\frac{3}{2} kT}}$, and $E_0 \equiv E_{\text{av}}(0)$ is the initial energy of Ps.

Figure 3 shows the best fit result of the previous experimental data from Ref. [1] considering nonlinear material effect using Equations (7) and (9) with parameters $E_0 = 2.07$ eV and $\sigma_m = 13.0 \text{ \AA}^2$ [11], compared with linear fitting. The nonlinear effect can be clearly seen at low density, and it can explain the discrepancy between $\Delta_{\text{HFS}}^{\text{exp}}$ and $\Delta_{\text{HFS}}^{\text{th}}$ (the best fit value including nonlinear effect is $\Delta_{\text{HFS}} = 203.39280(95)$ GHz). But $\sigma_m = 37 \pm 10 \text{ \AA}^2$ from Ref. [9], which is not consistent with the value of Ref. [11], affects only about 5 ppm and cannot explain the discrepancy. Therefore, new independent measurement of Ps thermalization is needed.

2.3. Our new methods

Our new methods will significantly reduce the systematic errors present in previous experiments; the Ps thermalization effect and the non-uniformity of the magnetic field. The main improvements in our experiment are the large bore superconducting magnet, β -tagging system, and high performance γ -ray detectors. Details are discussed in the following sections.

3. Prototype Run

The prototype run of the measurement with new methods has been performed.

3.1. Experimental Setup

A schematic diagram of the experimental setup of the prototype run is shown in Figure 4.

3.1.1. Large bore superconducting magnet

A large bore superconducting magnet is used to produce the magnetic field $B \sim 0.866$ T which induces the Zeeman splitting. The bore diameter of the magnet is 800 mm, and its length

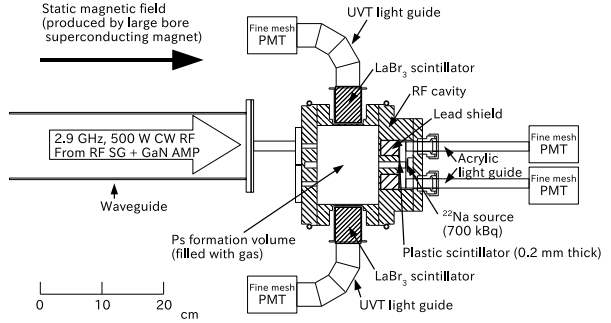


Figure 4: Schematic diagram of the experimental setup of the prototype run (top view in magnet).

is 2 m. The large bore diameter means that there is good uniformity in the magnetic field in the region where Ps is formed. Furthermore, the magnet is operated in persistent current mode, making the stability of the magnetic field better than ± 1 ppm.

The magnetic field distribution was measured using a proton NMR magnetometer (ECHO Electronics EFM-150HM-AX) with a clock synthesizer (NF Corporation CK1615 PA-001-0312). Calibration uncertainty of the system is less than 1 ppm. Non-uniformity of the magnetic field in a whole volume of RF cavity is 23.1 ppm (RMS) without any compensation coils. The non-uniformity decreases to 10.4 ppm when weighted by RF power and positron stop position distribution.

3.1.2. β -tagging system and timing information

The positron source is $19 \mu\text{Ci}$ (700 kBq) of ^{22}Na (Eckert & Ziegler POSN-22). A plastic scintillator (NE102A) 10 mm in diameter and 0.2 mm thick is used to tag positrons emitted from the ^{22}Na . The scintillation light is detected by fine mesh photomultiplier tubes (PMT: HAMAMATSU H6614-70MOD) and provides a start signal which corresponds to the time of Ps formation. The timing resolution is 1.0 ns (1σ). The positron then enters the microwave cavity, forming Ps in the gas contained therein.

Ps decays into photons that are detected with LaBr_3 (Ce) scintillators (Saint-Gobain BrilLanCeTM 380). Accumulating measurements of the times of positron emission and γ -detection results in decay curves of Ps as shown in Figure 5. The timing information is used to improve the accuracy of the measurement of Δ_{HFS} as follows:

1. Imposing a time cut means that we can select well thermalized Ps, reducing the unthermalized o-Ps contribution. It should also be possible to precisely measure the contributions of unthermalized o-Ps, and of material effects (we plan to make such measurements in future runs).
2. A time cut also allows us to avoid the prompt peak (contributions of simple annihilation and of fast p-Ps decay), which greatly increases the S/N of the measurement (by about a factor of 20).

3.1.3. High performance γ -ray detectors

Six γ -ray detectors are located around the microwave cavity to detect the 511 keV annihilation γ -rays. LaBr_3 scintillators, 1.5 inches in diameter and 2 inches long are used. The scintillation light is detected by fine mesh PMT through the UVT light guide. Without light guide, LaBr_3 scintillators have good energy resolution (4% FWHM at 511 keV) and timing resolution (0.2 ns FWHM at 511 keV), and have a short decay constant (16 ns). The good energy resolution and the high counting rate of LaBr_3 results in very good overall performance for measuring Zeeman transitions. In particular the good energy resolution allows us to efficiently separate 2γ events from 3γ events, negating the need to use a back-to-back geometry to select 2γ events, thus greatly increasing the acceptance of our setup.

This γ -ray detector system greatly reduces the statistical error in the measurement.

3.1.4. RF system

Microwaves are produced by a local oscillator signal generator (ROHDE & SCHWARZ SMV 03) and amplified to 500 W with a GaN amplifier (R&K A2856BW200-5057-R).

The microwave cavity is made with oxygen-free copper; the inside of the cavity is a cylinder 128 mm in diameter and 100 mm long. The side wall of the cavity is only 2 mm thick in order to allow the γ -rays to efficiently escape. The cavity is operated in the TM_{110} mode. The resonant frequency is 2.8566 GHz and $Q_L = 14,700 \pm 50$. The cavity is filled with gas (90% N_2 and 10% iso- C_4H_{10}) with a gas-handling system. Iso- C_4H_{10} is used as the quenching gas to remove background 2γ -ray annihilation.

3.1.5. Monte Carlo simulation

The Monte Carlo simulation to use in analysis is performed using Geant4 [12]. The low energy physics package PENELOPE [13] is used and the geometry of the experimental setup is carefully input. The simulation is produced at each magnetic field strength and gas density.

3.1.6. Data acquisition

The prototype run was performed from 2 July 2009 to 24 September 2009 using the large bore magnet with no compensation (compensation magnets to reduce the uniformity to O(ppm) are planned but are not yet installed). In the overall period, the trigger rate was about 3.6 kHz and the data acquisition rate was about 650 Hz. The data acquisition was performed using NIM and CAMAC system.

The trigger signal is the coincidence signal of β -tagging system and γ -ray detectors. Timing information of all PMT are obtained with a 2 GHz direct clock counting Time-to-Digital Converter (TDC: GNC-060) [4, 5]. A charge ADC (CAEN C1205) is used to measure the energy information of the LaBr_3 crystals while another charge ADC is used to measure the energy information of the plastic scintillators. A crate controller (TOYO CC/NET) is used and obtained data are stored in a HDD of a Linux PC via Ethernet. The Zeeman transition has been measured at various magnetic field strengths with a fixed RF fre-

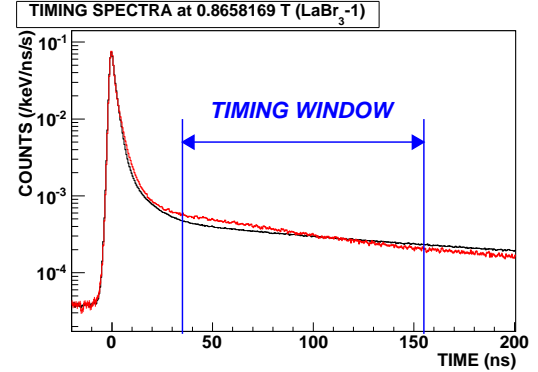


Figure 5: (Color online) Decay curves of Ps. The red line is on-resonance (0.865 8169 T) RF ON, and the black line is RF OFF. The timing window of 35–155 ns is also indicated. The decay rate of Ps increases with RF because of the Zeeman transition.

quency and power. The transition resonance lines are obtained at two gas densities (1.350 1 amagat and 0.891 6 amagat).

3.2. Analysis

3.2.1. Data analysis

Figure 5 shows examples of measured timing spectra. The prompt peak coming from annihilation and $|-\rangle$ decay is followed by the decay curve of $|+\rangle$ and $m_z = \pm 1$ states, then the constant accidental spectrum. A timing window of 35–155 ns is applied to select transition events. Figure 6 shows energy spectra, which are obtained by subtracting the accidental contribution using the timing window $t = 700$ –850 ns.

The energy spectra are fitted using Monte Carlo simulation. The energy spectrum of RF-OFF S_{OFF} can be expressed as

$$S_{\text{OFF}} = A_{\text{OFF}} (S_{3\gamma}^{\text{MC}} + \beta S_{2\gamma}^{\text{MC}}), \quad (10)$$

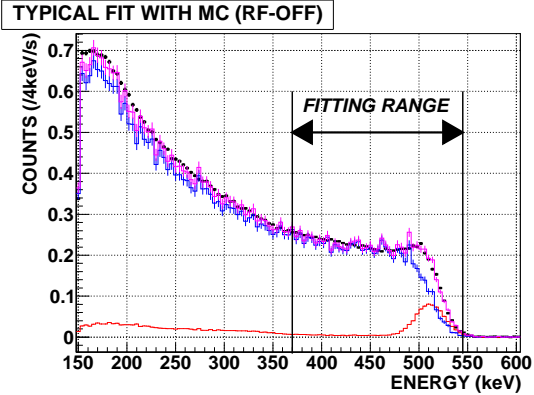
where A_{OFF} is a normalizing constant, β is a $2\gamma/3\gamma$ decay ratio of RF-OFF, $S_{2\gamma}^{\text{MC}}$ is a Monte Carlo simulated energy spectrum of 2γ decay, and $S_{3\gamma}^{\text{MC}}$ is that of 3γ decay. On the other hand, the energy spectrum of RF-ON S_{ON} can be expressed as

$$S_{\text{ON}} = A_{\text{ON}} (S_{3\gamma,\text{in}}^{\text{MC}} + \Gamma S_{2\gamma,\text{in}}^{\text{MC}}) + A_{\text{OFF}} (S_{3\gamma,\text{out}}^{\text{MC}} + \beta S_{2\gamma,\text{out}}^{\text{MC}}), \quad (11)$$

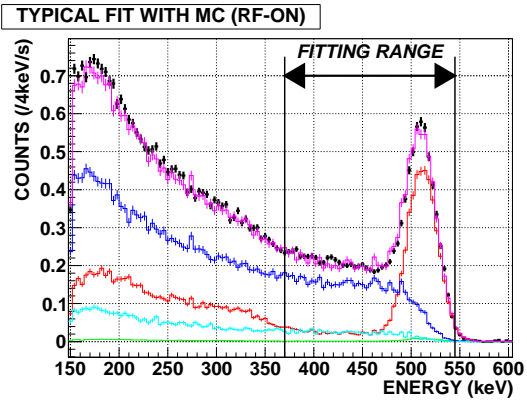
where A_{ON} is a normalizing constant and Γ is a $2\gamma/3\gamma$ decay ratio of RF-ON. The subscript “in” and “out” means the spectrum of γ -rays from Ps decays in the volume where RF power is applied or not applied, respectively.

Typical fitted results are also shown in Figure 6. Figure 6(a) is RF-OFF, and 6(b) is RF-ON. The energy spectrum is measured at different magnetic field strengths. The fitting range is 370–545 keV. All the spectra are fitted successfully using MINUIT [14].

We take $\Gamma - \beta$ as an amount of Zeeman transition. An example of resonance line obtained is shown in Figure 7. Resonance lines can be fitted by $S_{2\gamma}/S_{3\gamma}(\text{RF-ON}) - S_{2\gamma}/S_{3\gamma}(\text{RF-OFF})$. The theoretical function is calculated from Equations (5) and (6) numerically using RKF45 formula, with contributions from pick-off and slow positron. The typical B_0 is 14.2 G. The RF-OFF function is obtained by substitute 0 for B_0 . Then the free



(a) Typical fitting of energy spectrum (RF-OFF). The black points are the data, the red line is $S_{2\gamma}^{MC}$, the blue line is $S_{3\gamma}^{MC}$, and the pink line is sum of the Monte Carlo spectra.



(b) Typical fitting of energy spectrum (RF-ON). The black points are the data, the red line is $S_{2\gamma,in}^{MC}$, the blue line is $S_{3\gamma,in}^{MC}$, the green line is $S_{2\gamma,out}^{MC}$, the aqua line is $S_{3\gamma,out}^{MC}$, and the pink line is sum of the Monte Carlo spectra. A_{OFF} and β are fixed with the fitted values of RF-OFF, so that the free parameters are A_{ON} and Γ .

Figure 6: (Color online) Typical energy spectra and its fitting with Monte Carlo simulation. The data at 1.350 1 amagat, 0.865 816 9 T are shown and the spectra are normalized by the live time.

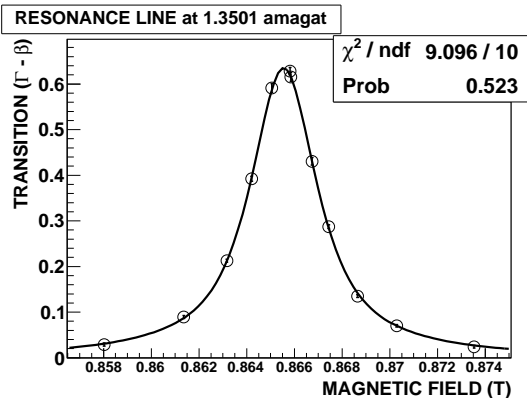


Figure 7: Resonance line at 1.350 1 amagat gas density. The circles and error bars are the data, and the solid line is the best fit result. The error bars include errors from statistics of data, statistics of Monte Carlo simulation, uncertainty of RF power, and uncertainty of Q_L value of the RF cavity.

Table 1: Fitting result of the resonance lines. These uncertainties include errors from statistics of data, statistics of Monte Carlo simulation, uncertainty of RF power, and uncertainty of Q_L value of the RF cavity.

Gas density (amagat)	Δ_{HFS} (GHz)	Relative error (ppm)	χ^2/ndf
1.350 1(71)	203.368 3(55)	27	0.910
0.891 6(23)	203.379 3(70)	34	0.483

parameters of fitting are Δ_{HFS} and C_y . The fitting results are summarized in Table 1. We use -33 ppm/amagat [1] as the material effect and obtain Δ_{HFS} in vacuum.

3.2.2. Systematic Errors

Systematic errors of the prototype run are summarized in Table 2.

1. *Magnetic Field.* The largest uncertainty in the prototype run is non-uniformity of the magnetic field. The weighted non-uniformity is 10.4 ppm. The offset and reproducibility of the magnetic field is measured to be 2 ppm. The calibration uncertainty of NMR magnetometer is 1 ppm. These uncertainties are doubled because Δ_{HFS} is approximately proportional to square of the magnetic field strength.
2. *Monte Carlo Simulation.* The magnetic field dependence of β is not exactly reproduced by the energy spectra fitting with Monte Carlo simulation. From the difference between theoretical dependence and fitted result, this effect is estimated to be 18 ppm. The statistical uncertainty of Monte Carlo simulation is 17 ppm.
3. *RF System.* The uncertainty of Q_L value of RF cavity comes from reproducibility of the RF environment ($\sim 5\%$) and uncertainty of the Q_L measurement method (0.6%). Its effect on Δ_{HFS} is estimated to be 6 ppm. RF power uncertainty comes from reproducibility of the RF environment ($\sim 2\%$), uncertainty of power meters (0.05%), and uncertainty of the power meter calibration of temperature dependence (0.03%/K). It contributes to the error on Δ_{HFS} by 5 ppm. The uncertainty of RF frequency is 5 ppm. It directly affects Δ_{HFS} because Δ_{HFS} is approximately proportional to inverse of RF frequency.
4. *Material Effect.* Thermalization of Ps can affect Δ_{HFS} by up to 20 ppm, but it has been not yet measured. Gas density dependence has not been measured in the prototype run, so we have used the value from previous experiment. The uncertainty of the density dependence is 4 ppm/amagat [1], and the uncertainty from iso-C₄H₁₀ is estimated to be less than 7.7 ppm/amagat. These result in 7 ppm uncertainty of Δ_{HFS} .

Other uncertainties are considered to be negligible. The systematic errors discussed above are summed in quadrature.

3.3. Result

The value of Δ_{HFS} obtained from the prototype run is

$$\Delta_{HFS} = 203.380 4 \pm 0.002 2(\text{stat.}, 11 \text{ ppm}) \\ \pm 0.008 1(\text{sys.}, 40 \text{ ppm}) \text{ GHz}, \quad (12)$$

Table 2: Summary of Systematic errors of the prototype run.

Source	Errors in Δ_{HFS} (ppm)
<i>Magnetic Field:</i>	
Non-uniformity	21
Offset and reproducibility	4
NMR measurement	2
<i>Monte Carlo Simulation:</i>	
Magnetic field dependence	18
Statistics	17
<i>RF System:</i>	
Q_L value of RF cavity	6
RF power	5
RF frequency	5
<i>Material Effect:</i>	
Thermalization of Ps	< 20
Gas density dependence	7
Quadrature sum	40

which is consistent with both of the previous experimental values and with the theoretical value. The uncertainty is an order of magnitude larger than the goal precision of O(ppm).

3.4. Next steps

The following improvements are planned for future measurements:

1. Compensation magnets will be installed and O(ppm) magnetic field uniformity is expected to be achieved.
2. The Monte Carlo simulation will be studied to reproduce the magnetic field dependence of energy spectra of Ps decays. Statistics of simulation will be reduced to O(ppm).
3. The errors from RF system will be reduced to O(ppm) by carefully controlling the environment (especially the temperature) of the experiment.
4. Measurements at various pressures of gas will be performed to estimate the material effect (the Stark effect). The accumulation of these measurements will result in an O(ppm) statistical error within a few years.
5. The timing information allows for a measurement of Ps thermalization as a function of time [4, 5, 6]. We can thus precisely measure the material effect including the thermalization effect.

4. Conclusion

A new experiment to measure the Ps-HFS which reduces possible common uncertainties in previous experiments has been constructed and the prototype run has been finished. A value of $\Delta_{\text{HFS}} = 203.3804 \pm 0.002\text{ (stat.)} \pm 0.008\text{ (sys.)}\text{ GHz}$ (41 ppm) has been obtained, which is consistent with both of the previous experimental values and with the theoretical calculation. Development of compensation magnets is underway with a view to obtaining O(ppm) magnetic field homogeneity for the final run. The final run will start soon. A new result with an accuracy of O(ppm) will be obtained within

a few years which will be an independent check of the discrepancy between the present experimental values and the QED prediction.

References

- [1] M. W. Ritter, P. O. Egan, V. W. Hughes, and K. A. Woodle, Phys. Rev. A 30 (1984) 1331.
- [2] A. P. Mills, Jr. and G. H. Bearman, Phys. Rev. Lett. 34 (1975) 246; A. P. Mills, Jr., Phys. Rev. A 27 (1983) 262.
- [3] B. A. Kniehl and A. A. Penin, Phys. Rev. Lett. 85 (2000) 5094; K. Melnikov and A. Yelkhovsky, Phys. Rev. Lett. 86 (2001) 1498; R. J. Hill, Phys. Rev. Lett. 86 (2001) 3280.
- [4] Y. Kataoka, S. Asai, and T. Kobayashi, Phys. Lett. B 671 (2009) 219.
- [5] Y. Kataoka, *Test of Bound State QED Higher Order Correction : Precision Measurement of Orthopositronium Decay Rate*, Ph. D. thesis (2007), the University of Tokyo; O. Jinnouchi, S. Asai, and T. Kobayashi, Phys. Lett. B 572 (2003) 117; O. Jinnouchi, *Study of Bound State QED : Precision Measurement of the Orthopositronium Decay Rate*, Ph. D. thesis (2001), the University of Tokyo.
- [6] S. Asai, S. Orito, and N. Shinohara, Phys. Lett. B 357 (1995) 475; S. Asai, *New Measurement of Orthopositronium Lifetime*, Ph. D. thesis (1995), the University of Tokyo.
- [7] H. Grotch and R. A. Hegstrom, Phys. Rev. A 4 (1971) 59; E. R. Carlson, V. W. Hughes, M. L. Lewis, and I. Lindgren, Phys. Rev. Lett. 29 (1972) 1059; H. Grotch, and R. Kashuba, Phys. Rev. A 7 (1973) 78; M. L. Lewis, and V. W. Hughes, Phys. Rev. A 8 (1973) 625.
- [8] A. H. Al-Ramadhan and D. W. Gidley, Phys. Rev. Lett. 72 (1994) 1632.
- [9] F. Saito, Y. Nagashima, and T. Hyodo, J. Phys. B36 (2003) 4191.
- [10] Y. Nagashima, T. Hyodo, K. Fujiwara, and A. Ichimura, J. Phys. B31 (1998) 329.
- [11] M. Skalsey, J. J. Engbrecht, C. M. Nakamura, R. S. Vallery, and D. W. Gidley, Phys. Rev. A67 (2003) 022504.
- [12] S. Agostinelli *et al.*, Nucl. Instr. and Meth. A 506 (2003) 250; J. Allison *et al.*, IEEE Trans. Nucl. Sci. 53 (2006) 270.
- [13] J. Baró *et al.*, Nucl. Instr. and Meth. B 100 (1995) 31.
- [14] IT/ASD CERN, *MINUIT Function Minimization and Error Analysis, version 94.1* D506 CERN Program Library.